

# A study of $\Lambda$ hypernuclei within the Skyrme-Hartree-Fock Model

Neelam Guleria<sup>a</sup>, Shashi K. Dhiman<sup>a,b</sup>, Radhey Shyam<sup>c,d</sup>

<sup>a</sup>*Department of Physics, H. P. University, Shimla 171005, India*

<sup>b</sup>*University Institute of Natural Sciences and Interface Technologies, Himachal Pradesh Technical University, Hamirpur 177001, India*

<sup>c</sup>*Saha Institute of Nuclear Physics, AF/1, Bidhan Nagar, Kolkata 700064, India*

<sup>d</sup>*Centre for the Subatomic Structure of Matter (CSSM), School of Chemistry and Physics, University of Adelaide, SA 5005, Australia*

---

## Abstract

We investigate the properties of the single  $\Lambda$  hypernuclei within a Skyrme-Hartree-Fock (SHF) model. The parameters of the Skyrme type effective lambda-nucleon ( $\Lambda N$ ) interaction are obtained by fitting to the experimental  $\Lambda$  binding energies of hypernuclei with masses spanning a wide range of the periodic table. Alternative parameter sets are also obtained by omitting nuclei below mass number 16 from the fitting procedure. The SHF calculations are performed for the binding energies of the  $\Lambda$  single-particle states over a full mass range using the best fit parameter sets obtained in these fitting procedures and the results are compared with the available experimental data. The data show some sensitivity to the parameter sets obtained with or without including the nuclei below mass 16. The radii of the  $\Lambda$  orbits in the hypernuclear ground states and the  $\Lambda$  effective mass in nuclear matter show some dependence on different parameter sets. We present results for the total binding energy per baryon of the hypernuclei over a large mass region to elucidate their stability as a function of the baryon number. We have also employed the our best fit  $\Lambda N$  parameter sets to investigate the role of hyperons in some key properties of neutron stars.

**Keywords:** Skyrme Hartree-Fock Model, Structure of Hypernuclei, Hyperon-nucleon effective interaction

**PACS:** 21.80.+q, 21.10.Dr, 21.30.Fe

---

## 1. Introduction

Hypernuclei provide an unique opportunity to investigate the dynamics of the full meson and baryon SU(3) flavor octet. They are an excellent tool to extract information on the hyperon-nucleon interaction. For a complete understanding of the baryon-baryon interactions in terms of the meson-exchange or quark-gluon pictures, the basic experimental data are required also on the hyperon-nucleon interaction together with the nucleon-nucleon interaction. Yet, relatively little is understood about nuclei that contain one or more hyperons. It is possible that the study of hypernuclei may help

in unraveling fundamental issues regarding the ordinary nuclei in terms of quantum chromodynamics (QCD) which is the theory of strongly interacting particles.

Since  $\Lambda$  is the lightest among the hyperons ( $m_\Lambda = 1.115$  GeV), the  $\Lambda$  hypernuclei are the most investigated systems so far [1, 2, 3, 4, 5, 6, 7, 8, 9]. Through a series of experimental studies involving  $(K^-, \pi^-)$ ,  $(\pi^+, K^+)$ ,  $(\gamma, K^+)$  and  $(e, e' K^+)$  reactions (see, e.g. Ref. [7] for a recent review of the experimental scenario) the  $\Lambda$  shell structure has been mapped out over a wide range of the periodic table. Systematic studies of the energy levels of light  $\Lambda$  hypernuclei have enabled the extraction of considerable amount of details about the  $\Lambda N$  interaction. It is established that the spin-orbit part of this force is weaker (see, e.g. Ref. [4] and the related references cite there) than that of the  $NN$  system. This has also been useful in developing the theoretical models of the hypernuclear production reactions where the quantum numbers and the binding energies of  $\Lambda$  single particle states are vital inputs [10, 11, 12, 13, 14, 15].

For several reasons it is necessary to have information about the behavior of a hyperon in nuclear medium which can be provided by the heavier  $\Lambda$  hypernuclei. The basic quantities like  $\Lambda$  effective mass and the depth of the  $\Lambda$  potential in nuclei can be obtained by investigating the  $\Lambda$  binding energies in a wide range of heavier systems. These quantities are the important basic parameters for a realistic discussion of neutron stars [16]. The information on the  $\Lambda$  spin-orbit splitting in heavier hypernuclei is of interest because it may have contributions from the higher order many body effects in addition to the  $\Lambda N$  two-body spin-dependent interaction.

It is therefore, important to develop reliable theoretical tools to investigate the spectroscopy of the hypernuclei. From QCD point of view hypernuclei lie in the non-perturbative low momentum regime. Therefore, lattice QCD calculations should be the ideal tool for investigating their structure. Indeed, first step in this direction has already been initiated where the scattering length and the effective range for  $\Lambda N$  scattering have been extracted in both QCD and partially-quenched QCD calculations [17]. However, a description of the detailed structure of hypernuclei is still beyond the reach of the lattice QCD and one has to use methods where baryons and mesons are the effective degrees of freedom.

Both relativistic and non-relativistic descriptions have been used to investigate the structure of hypernuclei. The relativistic mean field approach has been employed in Refs. [18, 19, 20, 21, 22] with meson-hyperon vertices adjusted in varied ways. The SU(3) symmetric field theories including chirality [23, 24], and the quark-meson coupling model [8, 25, 26] that invokes the quark degrees of freedom have been developed to investigate the structure of hypernuclei. A density dependent relativistic hadron (DDRH) field theory was used in Ref. [5] to describe  $\Lambda$  hypernuclei. In Ref. [9] a in-medium chiral SU(3) dynamics has been used to study the hypernuclear single particle spectra where a very good agreement has been achieved with the corresponding data. The smallness of the  $\Lambda$ -nuclear spin-orbit interaction also finds a natural explanation within this approach.

Among the non-relativistic approaches are the calculations based on the shell model picture (see, e.g., Ref. [27] for a review). Most of them reproduce reasonably well the measured hypernuclear states of medium to heavy hypernuclei using phenomenological  $\Lambda N$  potentials of the Woods-Saxon type [28, 29, 11]. Several authors have also developed the semi-empirical mass formulas to describe the binding energy (BE) of

the hypernuclei [30, 31, 32]

The Skyrme-Hartree-Fock (SHF) model, which has been a powerful tool for investigating the properties of nonstrange nuclei [33, 34, 35], was extended to studies of the  $\Lambda$  hypernuclei in Refs. [36, 37]. The suitability of this approach for describing the  $\Lambda$  hypernuclei depends heavily on the proper knowledge of the  $\Lambda N$  effective interaction, which has either been extracted from the microscopic methods like  $G$ -matrix calculations performed with Jülich and Nijmegen potentials [38, 39, 40, 41, 42, 43] or by fitting directly to the hypernuclear data (mainly the binding energies) [37, 44, 45]. The reliability of the latter method is related directly to the amount of hypernuclear data used in the fitting process. In previous studies, the data used for this purpose were limited to a few light nuclei. Therefore, there is a need to perform SHF calculations using the  $\Lambda N$  interaction with parameters that are determined by fitting to a larger set of data on binding energies that is available now.

In this paper, we study the  $\Lambda$  hypernuclei within the framework of the Hartree-Fock method where the parameters of the Skyrme type  $\Lambda N$  effective interaction have been determined by fitting to the experimental binding energies of hypernuclei with baryon numbers ranging over a wide mass range. In one fitting procedure, we have included nuclei with masses ranging between 8 to 208. In two more fittings, the nuclei with masses below 16 were omitted. We have also included a density dependent term in the  $\Lambda N$  interaction in our fitting procedure as suggested in Ref. [46, 47]. The parameter sets having the minimum  $\chi^2$  values in three searches have been used to calculate the binding energies of about 95 hypernuclear states and the results are compared with the available experimental data. Furthermore, we have also calculated the total binding energy per baryon of 73  $\Lambda$  hypernuclei, and the root mean square (RMS) radii of a few nuclei of them. Finally our best fit parameter sets have been used to investigate some properties of neutron stars.

The present paper is organized as following. In section II, the Skyrme-Hartree-Fock method as applied to the description of the single  $\Lambda$  hypernuclei, is briefly described and parameters involved in the Skyrme type  $\Lambda N$  force are discussed. In section III, we describe the  $\chi^2$  minimization method [based on the simulated annealing method (SAM)] that is used by us to determine the best fit parameters of the  $\Lambda N$  interaction. In section IV, we present the results and discussions of the comparison of our calculations for the single particle energies of the  $\Lambda$  states with the available experimental data. The results for the total binding energies per baryon of a larger number of single  $\Lambda$  hypernuclei are also presented in this section. We also investigate the role of our best fit  $\Lambda N$  interactions on some properties of neutron stars. Finally, in section V, we present the summary and conclusions of our work.

## 2. Formalism

The SHF model for nonstrange nuclei has been discussed in great details in Refs. [33, 34, 35]. In its extension [36, 37] to describe the  $\Lambda$  hypernuclei a contribution is added to the original energy density functional to account for the action of the hyperon-nucleon force. Thus, the total energy density functional (EDF) of a hypernucleus is written as a sum of two basic contributions -  $\mathcal{E}_N$ , which is the total energy density for neutron

and proton [33] and  $\mathcal{E}_\Lambda$ , which is the contribution due to the presence of the hyperon (hyperons):

$$\mathcal{E}_{1\Lambda}^H = \mathcal{E}_N(\rho_n, \rho_p, \tau_n, \tau_p, \mathbf{J}_n, \mathbf{J}_p) + \mathcal{E}_\Lambda(\rho_n, \rho_p, \rho_\Lambda, \tau_\Lambda), \quad (1)$$

where  $\rho_q$ ,  $\tau_q$  and  $J_q$  represent the baryon, kinetic and spin-orbit current densities, respectively ( $q = n, p, \Lambda$ ). There are some additional terms contributing to the total hypernuclear energy that will be discussed latter on in this section.

$\mathcal{E}_N$  is related to the original SHF nuclear Hamiltonian density ( $H_N$ ) as

$$\mathcal{E}_N = \int d^3r H_N(\mathbf{r}), \quad (2)$$

where  $H_N$  is written as [48, 49]

$$\begin{aligned} H_N = & \frac{\hbar^2}{2m} \tau_N + \frac{1}{4} t_0 [(2 + x_0) \rho_N^2 - (2x_0 + 1)(\rho_p^2 + \rho_n^2)] \\ & + \frac{1}{24} t_3 \rho^a [(2 + x_3) \rho_N^2 - (2x_3 + 1)(\rho_p^2 + \rho_n^2)] \\ & + \frac{1}{8} [t_1(2 + x_1) + t_2(2 + x_2)] \tau_N \rho_N + \frac{1}{8} [t_2(2x_2 + 1) - t_1(2x_1 + 1)] (\tau_p \rho_p + \tau_n \rho_n) \\ & + \frac{1}{32} [3t_1(2 + x_1) - t_2(2 + x_2)] (\nabla \rho_N)^2 - \frac{1}{32} [3t_1(2x_1 + 1) + t_2(2x_2 + 1)] [(\nabla \rho_p)^2 + (\nabla \rho_n)^2] \\ & + \frac{1}{2} W_0 [\mathbf{J}_N \cdot \nabla \rho_N + \mathbf{J}_p \cdot \nabla \rho_p + \mathbf{J}_n \cdot \nabla \rho_n] \\ & - \frac{1}{16} (t_1 x_1 + t_2 x_2) \mathbf{J}_N^2 + \frac{1}{16} (t_1 - t_2) [\mathbf{J}_p^2 + \mathbf{J}_n^2] \\ & + \frac{1}{2} e^2 \rho_p(r) \int \frac{\rho_p(r') d^3r'}{|\mathbf{r} - \mathbf{r}'|} - \frac{3}{4} e^2 \rho_p(r) \left( \frac{3\rho_p(r)}{\pi} \right)^{1/3}, \end{aligned} \quad (3)$$

where the first term on the right hand side represents the kinetic energy. We define,  $\rho_N = \rho_n + \rho_p$ ,  $\tau_N = \tau_n + \tau_p$  and  $J_N = J_n + J_p$ , where  $n(p)$  correspond to a neutron (proton). We employ SLy4 Skyrme parameterization [48] in the calculation of the energy density of the hypernuclear core  ${}_{\Lambda}^{A-1}Z$ . This interaction has been widely used in studies of the nuclear structure of normal and neutron rich nuclei [50], and the properties of nuclear matter and neutron stars [51].

The densities  $\rho_q$ ,  $\tau_q$  and  $J_q$  are expressed as

$$\rho_q(\mathbf{r}) = \sum_{\beta} v_{\beta} |\phi_{\beta}(\mathbf{r}, q)|^2, \quad (4)$$

$$\tau_q(\mathbf{r}) = \sum_{\beta} v_{\beta} |\nabla \phi_{\beta}(\mathbf{r}, q)|^2, \quad (5)$$

$$\mathbf{J}_q(\mathbf{r}) = \sum_{\beta} v_{\beta} \phi_{\beta}^*(\mathbf{r}, q) (-i \nabla \times \sigma) \phi_{\beta}(\mathbf{r}, q), \quad (6)$$

where  $\phi_{\beta}(\mathbf{r}, q)$  are the wave functions of the single particle states,  $v_{\beta}$  represents the occupation probability, and  $\sigma$  the Pauli spin matrices. The sums are taken over all

occupied states for different particles  $q$ . Summations over spin, and isospin indices are implicit.

The occupation probabilities  $v_\beta$  of neutrons and protons are calculated by including the pairing energy functional  $\mathcal{E}_{pair}$  in Eq. (1) as described in Ref. [50]. The BCS equations for the pairing probabilities are obtained by variational method with respect to  $v_\beta$  and written as,

$$v_\beta^2 = \frac{1}{2} \left[ 1 - \frac{\epsilon_\beta - \mu_\beta}{\sqrt{(\epsilon_\beta - \mu_\beta)^2 + \Delta_q^2}} \right], \quad (7)$$

where  $\epsilon_\beta$  is the single particle energy of the occupied state, and  $\mu_\beta$  is the chemical potential. The pairing gap equation has the form  $\Delta_q = G_q \sum_{\beta \in q} \sqrt{v_\beta(1 - v_\beta)}$ , where  $G_q$  is as defined in Ref. [50].

The energy density functional  $\mathcal{E}_\Lambda$  is written as

$$\mathcal{E}_\Lambda = \int d^3r H_\Lambda(\mathbf{r}). \quad (8)$$

As in Ref. [37],  $H_\Lambda$  in Eq. 8 has a term that corresponds to a Skyrme type two-body force,

$$\begin{aligned} H_\Lambda^{\Lambda N} &= \frac{\hbar^2}{2m_\Lambda} \tau_\Lambda + u_0 \left( 1 + \frac{1}{2} y_0 \right) \rho_N \rho_\Lambda \\ &+ \frac{1}{4} (u_1 + u_2) (\tau_\Lambda \rho_N + \tau_N \rho_\Lambda) + \frac{1}{8} (3u_1 - u_2) (\nabla \rho_N \cdot \nabla \rho_\Lambda) \\ &+ \frac{1}{2} W_\Lambda (\nabla \rho_N \cdot \mathbf{J}_\Lambda + \nabla \rho_\Lambda \cdot \mathbf{J}_N), \end{aligned} \quad (9)$$

In ref. [37] and [45], a second term is added to  $H_\Lambda$  that corresponds to a zero range three-body  $\Lambda NN$  force.

$$H_\Lambda^{\Lambda NN} = \frac{u_3}{4} \rho_\Lambda (\rho_N^2 + 2\rho_n \rho_p). \quad (10)$$

This is completely analogous to the corresponding term of the nucleon Skyrme force proposed in Ref. [33]. It has been pointed out in Refs. [52, 53, 54] that the binding energies of particularly light hypernuclei can be better reproduced if three-body  $\Lambda NN$  term is included in the calculations. For example the overbinding problem of  ${}^5_\Lambda\text{He}$  hypernucleus has been solved by taking into account the  $\Lambda NN$  force in Ref. [55]. In the Skyrme Hartree-Fock calculations of Ref. [45] it is shown that the inclusion this term leads to a better reproduction of the  $1p - 1d$  and  $1s - 1p$  levels spacings in several nuclei.

In the Hartree-Fock calculations of even-even nuclei, the three-body part of the Skyrme interaction is equivalent to a two-body density-dependent interaction [33, 35]. Therefore, some authors [46, 47] have included in  $H_\Lambda$  a term dependent on the nuclear density instead of the  $\Lambda NN$  force,

$$H_\Lambda^{\Lambda Np} = \frac{3}{8} u'_3 \left( 1 + \frac{1}{2} y_3 \right) \rho_N^{\gamma+1} \rho_\Lambda, \quad (11)$$

where  $\gamma$  and  $y_3$  are additional parameters. It may however, be remarked that at least for  $\gamma \neq 1$ , Eq. (11) can not be derived from any three-body force. Furthermore, the equivalence of three-body and the density dependent forces in the hypernuclear case is not exact even for  $\gamma = 1$ . In the limit of  $\gamma = 1$  and  $y_3 = 0$ , Eq. (11) does reduce to a form similar (but not strictly equal) to Eq. (10). Nevertheless, using Eq. (11) leads to a value of nuclear incompressibility that is closer to its experimental value [47]. It is stated in Ref. [46] that Eq. (10) is not so adequate for representing the density dependence of the  $\Lambda N$   $G$  matrix while Eq. (11) with a value of  $\gamma = \frac{1}{3}$  is good enough for parameterizing the  $G$  matrix result. Therefore, in our calculations we have added Eq. (11) to the Hamiltonian instead of the three-body force term, Eq. (10), and have considered for  $\gamma$  both 1 and  $\frac{1}{3}$ . We have used  $\hbar^2/2m_\Lambda = 17.44054 \text{ MeV fm}^2$ .

Now, the single-particle wave functions  $\phi_\beta(\mathbf{r}, q)$  and corresponding single-particle energies  $\epsilon_\beta$  are obtained by solving the Hartree-Fock equations with position and density dependent mass term

$$\left[ -\nabla \frac{\hbar^2}{2m_q^*} \cdot \nabla + V_q(\mathbf{r}) - iW_q(\mathbf{r}) \cdot (\nabla \times \sigma) \right] \phi_\beta(\mathbf{r}, q) = \epsilon_\beta \phi_\beta(\mathbf{r}, q), \quad (12)$$

where  $m_q^*$  is the effective baryon mass, and  $V_q$  and  $W_q$  are the central and spin-orbit terms of the mean field potential, respectively. The central term consists of (i) a purely nuclear part ( $V_{NN}$ ) as described, e.g., in Refs. [33, 48], (ii) additional field created by the  $\Lambda$  hyperon ( $V_N^\Lambda$ ) that is seen by a nucleon, and (iii) the whole nuclear field experienced by the  $\Lambda$  hyperon ( $V_\Lambda^\Lambda$ ). The effective mass of the nucleon will also have additional terms. The spin-orbit part of the  $\Lambda N$  interaction has been ignored ( $W_\Lambda = 0$ ) from the start as is done in Ref. [37]. The smallness of this term has been supported by several microscopic calculations [56, 57, 25]. The potentials  $V_\Lambda^\Lambda$  and  $V_N^\Lambda$  are written as

$$\begin{aligned} V_\Lambda^\Lambda &= u_0(1 + \frac{1}{2}y_0)\rho_N + \frac{1}{4}(u_1 + u_2)(\nabla \tau_\Lambda \rho_N + \tau_N) \\ &+ \frac{1}{8}(3u_1 - u_2)(\nabla^2 \rho_N) - \frac{1}{4}(3u_1 - u_2)(\nabla \rho_N/r) + \frac{3}{8}u'_3(1 + \frac{1}{2}y_3)\rho_N^{\gamma+1}, \end{aligned} \quad (13)$$

and,

$$\begin{aligned} V_N^\Lambda &= u_0(1 + \frac{1}{2}y_0)\rho_\Lambda + \frac{1}{4}(u_1 + u_2)(\tau_\Lambda + \nabla \tau_N \rho_\Lambda) + \frac{1}{8}(3u_1 - u_2)(\nabla^2 \rho_\Lambda) \\ &- \frac{1}{4}(3u_1 - u_2)(\nabla \rho_\Lambda/r) + \frac{3}{8}u'_3(1 + \frac{1}{2}y_3)(\gamma + 1)\rho_N^\gamma \rho_\Lambda. \end{aligned} \quad (14)$$

The spin-orbit part of the mean field has purely nucleonic contribution and it can be written in a straight forward standard way.

The term containing the effective mass of the single  $\Lambda$  hyperon is expressed as,

$$\frac{\hbar^2}{2m_\Lambda^*} = \frac{\hbar^2}{2m_\Lambda} + \frac{1}{4}(u_1 + u_2)\rho_N. \quad (15)$$

Similarly, the effective mass term for nucleon (in presence of a hyperon) is written as

$$\frac{\hbar^2}{2m_{q^*}} = \frac{\hbar^2}{2m_{q'}} + \frac{1}{8}[t_1(2+x_1) + t_2(2+x_2)]\rho_N + \frac{1}{8}[t_2(2x_2+1) - t_1(2x_1+1)]\rho_{q'} + \frac{1}{4}(u_1 + u_2)\rho_\Lambda, \quad (16)$$

where  $q'$  represents a nucleon (neutron or proton). The potentials, the effective masses, and the orbitals in Eq. (12) are evaluated alternatively until self-consistency is achieved.

The total hypernuclear energy, in a density dependent Hartree-Fock model, includes contributions also from the  $H_{NNN}$  and  $H_{\Lambda N}^p$  terms. Our total energy due to nucleon terms only includes relevant contributions. For the  $\Lambda$  case, we have

$$\mathcal{E}_R^\Lambda = \frac{3}{16} u'_3 \int d^3r \left(1 + \frac{1}{2} y_3\right) \rho_N^{\gamma+1} \rho_\Lambda \quad (17)$$

We also have to introduce to the total energy the center of mass (c.m.) correction arising due to the breaking of the translational invariance in the mean field of the Hartree-Fock theory. This is written as

$$\mathcal{E}_{c.m.} = \frac{\langle P_{c.m.}^2 \rangle}{2(A-n)m_N + nm_\Lambda}, \quad (18)$$

where  $m_N$  and  $m_\Lambda$  are the masses of nucleon and  $\Lambda$  hyperon, respectively while  $n$  denotes the number of lambda particles (in our case  $n=1$ ), and  $A$  is the baryon number of the hypernucleus.  $P_{c.m.} = \sum_k \hat{p}_k$  is the total momentum operator in the c.m. frame, which is the sum of the single particle momentum operators ( $\hat{p}_k$ ). Although the BCS state is not an eigenstate of  $\hat{P}_{c.m.}$ , and has vanishing total momentum  $\langle \hat{P}_{c.m.} \rangle = 0$ , it has non-vanishing expectation value of  $\langle P_{c.m.}^2 \rangle$  given by,

$$\langle P_{c.m.}^2 \rangle = \sum_\alpha v_\alpha^2 \langle \alpha\alpha | \mathbf{p}^2 | \alpha\alpha \rangle \quad (19)$$

$$- \sum_{\alpha\beta} v_\alpha v_\beta (v_\alpha v_\beta - u_\alpha u_\beta) \langle \alpha\beta | \mathbf{p}_1 \cdot \mathbf{p}_2 | \alpha\beta \rangle, \quad (20)$$

where  $u_\alpha = \sqrt{1 - v_\alpha^2}$ , and  $\alpha$  and  $\beta$  represent the single particle states. This correction, however, is computed after variation (i.e., *posteriori*). The square of the single particle momentum operator appear only in the direct term of the c.m. correction. The second and third terms represent the off diagonal single particle matrix elements of the momentum operators that result from the exchange terms in  $\langle P_{c.m.}^2 \rangle$ . The c.m. energy correction due to hyperons is approximated by the diagonal part of the c.m. kinetic energy only.

Thus, the total hypernuclear energy is given by the expression

$$\mathcal{E}_{1\Lambda}^H = \mathcal{E}_N(\rho_n, \rho_p, \tau_n, \tau_p, \mathbf{J}_n, \mathbf{J}_p) + \mathcal{E}_{pair}(v_p, v_n) + \mathcal{E}_\Lambda(\rho_n, \rho_p, \rho_\Lambda, \tau_\Lambda) - \mathcal{E}_R^\Lambda - \mathcal{E}_{c.m.}, \quad (21)$$

where  $\mathcal{E}_{pair}(v_p, v_n)$  is the pairing energy density functional as described above.

The  $\Lambda$  binding energy in the SHF formalism is defined as

$$B_\Lambda = \mathcal{E}_N^0 - \mathcal{E}_{1\Lambda}^H, \quad (22)$$

where  $\mathcal{E}_{1\Lambda}^H$  and  $\mathcal{E}_N^0$  are the total binding energies of the hypernucleus and the core nucleus, respectively and binding energy per baryon number is obtained by dividing  $B_\Lambda$  with  $A$  (baryon number).

The fitting procedure to obtain the parameters of the  $\Lambda N$  interaction is described in the next section.

Table 1: Experimental values of the binding energies (in MeV) of various hypernuclei used in the  $\chi^2$  minimization procedure.

Hypernuclei	1s	BE(Expt.) 1p	1d
$^8_\Lambda\text{He}$ [59]	$7.16 \pm 0.70$	$7.0 \pm 0.2$	
$^9_\Lambda\text{Li}$ [59]	$8.50 \pm 0.12$		
$^{10}_\Lambda\text{Be}$ [59]	$9.11 \pm 0.22$		
$^{10}_\Lambda\text{B}$ [60, 61, 59]	$8.89 \pm 0.12$		
$^{11}_\Lambda\text{B}$ [59, 62]	$10.24 \pm 0.05$		
$^{12}_\Lambda\text{B}$ [59, 63]	$11.37 \pm 0.06$		
$^{12}_\Lambda\text{C}$ [64]	$10.76 \pm 0.19$		
$^{13}_\Lambda\text{C}$ [65, 66]	$11.69 \pm 0.12$		
$^{16}_\Lambda\text{N}$ [67]	$13.76 \pm 0.16$		
$^{16}_\Lambda\text{O}$ [68, 69]	$12.50 \pm 0.35$		
$^{28}_\Lambda\text{Si}$ [7, 61]	$16.60 \pm 0.20$		
$^{32}_\Lambda\text{S}$ [70]	$17.50 \pm 0.50$		
$^{40}_\Lambda\text{Ca}$ [71, 72]	$18.70 \pm 1.1$		
$^{51}_\Lambda\text{V}$ [73, 64]	$19.90 \pm 1.0$		
$^{89}_\Lambda\text{Y}$ [7, 64]	$23.10 \pm 0.50$	$16.50 \pm 4.1$	$9.1 \pm 1.3$
$^{139}_\Lambda\text{La}$ [7]	$24.50 \pm 1.20$	$20.4 \pm 0.6$	$14.3 \pm 0.6$
$^{208}_\Lambda\text{Pb}$ [7]	$26.30 \pm 0.80$	$21.90 \pm 0.6$	$16.8 \pm 0.7$

### 3. Parameterization for $\Lambda\text{N}$ Skyrme Potential

The values of parameters  $u_0$ ,  $u_1$ ,  $u_2$ ,  $u'_3$ ,  $y_0$  and  $y_3$  have been determined by fitting to the experimental binding energies (BE) of a set of hypernuclei across the periodic table by a  $\chi^2$  minimization procedure that is based on the SAM. This is an elegant technique of searching for a global minimum in the hypersurface of the  $\chi^2$  functions, which depend on the values of the parameters of the Skyrme interaction [58]. This method has been used in Ref. [49] to determine the parameters of the Skyrme type nucleon-nucleon effective interaction, which have been used to describe successfully the properties of normal and neutron rich nuclei as well as those of neutron stars.

The  $\chi^2$  function is defined as

$$\chi^2 = \frac{1}{N_d - N_p} \sum_{i=1}^{N_d} \left( \frac{M_i^{exp} - M_i^{th}}{\sigma_i} \right)^2, \quad (23)$$

where  $N_d$  is the numbers of the experimental data points and  $N_p$  the number of fitted parameters.  $\sigma_i$  stands for the theoretical error and  $M_i^{exp}$  and  $M_i^{th}$  are the experimental and the corresponding theoretical values, respectively, of a given observable (which in this case is the binding energy). The values of  $\chi^2$  depend on the Skyrme parameters being searched [in our case  $u_0$ ,  $u_1$ ,  $u_2$ ,  $u'_3$ ,  $y_0$  and  $y_3$  appearing in Eqs. (9) and (11)], since  $M_i^{th}$  is calculated using potentials with these parameters. Although there are correlations in some of these parameters (e.g.  $u_0$ ,  $y_0$ , and  $u'_3$ ,  $y_3$ ), we have varied



Table 2: The lower ( $\mathbf{v_0}$ ) and upper ( $\mathbf{v_1}$ ) limits, maximum displacement ( $\mathbf{d}$ ) and initial values ( $\mathbf{v_{in}}$ ) for the Skyrme force parameters used for implementing the SAM algorithm for minimizing the  $\chi^2$  value that leads to the parameter set (HPA2) to be shown in Table 3 .

Parameter	$\mathbf{v_0}$	$\mathbf{v_1}$	$\mathbf{d}$	$\mathbf{v_{in}}$
$u_0(\text{MeV } fm^3)$	-592	-275	2.0	-346
$u_1(\text{MeV } fm^5)$	0	100	1.0	60
$u_2(\text{MeV } fm^5)$	0	100	1.0	50
$u'_3(\text{MeV } fm^{3+3\gamma})$	1850	2300	3.0	1620
$y_0$	-0.7	-0.05	0.01	-0.13
$y_3$	-1.5	-0.01	0.01	-0.38

Table 3: Parameters for the  $\Lambda\text{N}$  Skyrme potential derived self-consistently by fitting to the experimental binding energies of table I for two different values of  $\gamma$ .

SET	$\gamma$	$u_0$ (MeV $fm^3$ )	$u_1$ (MeV $fm^5$ )	$u_2$ (MeV $fm^5$ )	$u'_3$ (MeV $fm^{3+3\gamma}$ )	$y_0$	$y_3$	$\chi^2$
HPA1	1	-326.395	72.627	-8.584	1746.041	-0.223	-0.389	3.58
HPA2	1	-399.946	83.426	11.455	2046.818	-0.486	-0.660	3.06
HPA3	1/3	-498.515	65.203	19.001	995.832	-0.492	-0.444	3.69
HPA4	1/3	-475.584	99.058	-20.890	1375.172	-0.350	-0.724	3.76

each one them independently - minimization of the  $\chi^2$  was the only requirement of our procedure. This is in complete analogy with the procedure of Refs. [58, 49]. The theoretical errors (see, Eq. 23) in the fitting algorithm are taken to be equivalent to the experimental uncertainty in the data.

The SAM is an elegant technique for optimization problems of large scale, in particular, where a desired global extremum is hidden among many local extrema. This method has been found to be an extremely useful tool for a wide variety of minimization problems of large non-linear systems in many different fields (e.g., see, Refs. [74, 75, 76]). Recently, the SAM was used to generate some initial trial parameter sets for the point coupling variant of the relativistic mean field model [77, 78].

In the SAM one needs to specify the appropriate annealing schedule together with the parameter space (i.e., the range of the values of the parameters) in which the best fit parameters are to be searched. As in Ref. [49], we have employed a moderately faster Cauchy annealing schedule given by

$$T(k) = T_i/k, \quad (24)$$

where  $T_i$  is the initial value of the control parameter and  $T(k)$ , with  $k=1,2,3,\dots$ , is the control parameter at the  $k$ th step. The value of  $k$  is increased by unity after  $120N_p$  reconfigurations or  $12N_p$  successful reconfigurations, whichever occurs first. The value of  $T_i$  is taken to be 5.0, which is the same as that used in Ref. [49]. We keep on reducing the value of the control parameter using Eq. (24) in the subsequent steps until  $\chi^2$  becomes stationary with further reduction. Since in our case number of parameters

Table 4: Experimental binding energy (in MeV) of various states of known single lambda hypernuclei with masses  $\geq 16$  used in the alternative fitting procedure.

Hypernuclei	1s	1p	BE(Expt.) 1d	1f	1g
$^{16}_{\Lambda}\text{N}$	$13.76 \pm 0.16$	$2.84 \pm 0.16$			
$^{16}_{\Lambda}\text{O}$	$12.50 \pm 0.35$	$1.85 \pm 0.05$			
$^{28}_{\Lambda}\text{Si}$	$16.60 \pm 0.20$	$7.0 \pm 0.2$			
$^{32}_{\Lambda}\text{S}$	$17.50 \pm 0.50$				
$^{40}_{\Lambda}\text{Ca}$	$18.70 \pm 1.1$				
$^{51}_{\Lambda}\text{V}$	$19.97 \pm 0.13$	$11.28 \pm 0.6$			
$^{89}_{\Lambda}\text{Y}$	$23.10 \pm 0.50$	$16.50 \pm 4.1$	$9.1 \pm 1.3$	$2.3 \pm 1.2$	
$^{139}_{\Lambda}\text{La}$	$24.50 \pm 1.20$	$20.4 \pm 0.6$	$14.3 \pm 0.6$	$8.0 \pm 0.6$	$1.5 \pm 0.6$
$^{208}_{\Lambda}\text{Pb}$	$26.30 \pm 0.80$	$21.90 \pm 0.6$	$16.8 \pm 0.7$	$11.7 \pm 0.6$	$6.6 \pm 0.6$

to be searched is rather large, we have defined the parameter space directly in terms of the range of values each parameter can take. Therefore, one of the key ingredients required for implementing SAM, in the present case, is to specify lower and upper limits for each of the parameter so that minimum is searched within these limits. In Table 2, we give some details of this procedure for one of the parameter sets to be shown in Table 3 that leads to the lowest  $\chi^2$ . In this table, lower and upper limits of the values of the Skyrme parameters are denoted by  $\mathbf{v}_0$  and  $\mathbf{v}_1$  in each case, respectively. In the third column,  $\mathbf{d}$  represents the maximum displacement allowed in a single step for a given Skyrme parameter during the reconfiguration process (see Refs. [49] and [58] for more details).  $\mathbf{v}_{\text{in}}$ , in the last column, shows the initial values of the Skyrme parameters used as a starting point for the SAM.

We first applied this procedure to fit the BE data listed in Table 1. In our search procedure, we used two values for the parameter  $\gamma$ , 1 and  $\frac{1}{3}$ . For each  $\gamma$ , 2 parameter sets, generated by following the fitting procedure discussed above, are shown in Table 3. The  $\chi^2$  values for each set is given in the last column of this table. Sets HPA1 and HPA2 have  $\gamma = 1$  while HPA3 and HPA4 have  $\gamma = \frac{1}{3}$ . We note that parameter set HPA2 has the lowest  $\chi^2$  value among of all the sets. With  $\gamma = \frac{1}{3}$ , set HPA3 provides the lowest  $\chi^2$ . We have used the set HPA2 in further calculations of the hypernuclear properties unless specified otherwise. In neutron star studies, however, the set HPA3 has also been used. The different sets of parameters shown in Table 3, lead to a depth of the  $\Lambda\text{N}$  mean field of about  $28.00 \pm 0.58$  MeV at the nuclear matter density ( $\rho_0$ ) of  $0.16 \pm 0.01 \text{ fm}^{-3}$ .

It could, however, be argued that hypernuclei with baryon number below 16 are too light to be used in the Skyrme Hartree-Fock fitting procedure, even through the Hartree-Fock method itself has been used to calculate the properties of light nuclei like He and Be by several authors (see, e.g. Ref. [93] and [41]). We have, therefore, also performed our fitting procedure by excluding all the nuclei with masses less than 16. Furthermore, since, experimental binding energies of  $1f$  orbit in  $^{89}_{\Lambda}\text{Y}$  and  $1f$  and  $1g$  orbits in  $^{139}_{\Lambda}\text{La}$  and  $^{208}_{\Lambda}\text{Pb}$  are also available (see, e.g., Refs. [64, 7]), we have included them also in

Table 5: Parameters for the  $\Lambda N$  Skyrme potential derived self-consistently by fitting to the experimental binding energies of table 4 for two different values of  $\gamma$ . The sets NA1 and NA2 are obtained by including the BEs of  ${}_{\Lambda}^{16}\text{N}$  and those of the rest of the nuclei but excluding the BE of  ${}^{16}\text{O}$  while OA1 and OA2 corresponds to the fits achieved by including BEs of  ${}_{\Lambda}^{16}\text{O}$  and the rest but excluding the BE of  ${}^{16}\text{N}$

SET	$\gamma$	$u_0$ (MeV fm <sup>3</sup> )	$u_1$ (MeV fm <sup>5</sup> )	$u_2$ (MeV fm <sup>5</sup> )	$u'_3$ (MeV fm <sup>3+3<math>\gamma</math>)</sup>	$y_0$	$y_3$	$\chi^2$
NA1	1	-253.3250	147.1264	-83.5843	1684.9876	0.5802	0.4831	2.30
OA1	1	-236.5835	116.8704	-112.8812	1453.3493	0.1271	-0.3110	1.82
NA2	1/3	-518.620	82.0944	-19.9772	1190.1894	-0.1392	0.3126	2.51
OA2	1/3	-417.7593	1.5460	-3.2617	1102.2221	-0.3854	-0.5645	1.92

our this alternative fitting. The BEs of the  $1s$  and  $1p$  levels of the hypernucleus  ${}_{\Lambda}^{16}\text{N}$  have recently become available from the study of the  $(e, e'K)$  reaction in the Jefferson Laboratory [67] while those for the  ${}_{\Lambda}^{16}\text{O}$  hypernucleus are given in Ref. [73]. These binding energies together with those of the other heavier hypernuclear systems are shown in table 4.

We have performed two sets of fits - one by including BE data of the  ${}_{\Lambda}^{16}\text{N}$  hypernucleus together with those the rest of the nuclei shown in table 4 but excluding the  ${}^{16}\text{O}$  data, and the another where the BE data of  ${}^{16}\text{O}$  system are included but those of  ${}^{16}\text{N}$  are excluded. The resulting parameters having the minimum  $\chi^2$  values, are shown in table 5 with *gamma* parameter of 1 and 1/3. The parameter sets NA1 and NA2 include the binding energies of  ${}_{\Lambda}^{16}\text{N}$  while OA1 and OA2 include those of  ${}_{\Lambda}^{16}\text{O}$ . We note from table 5 that the minimum  $\chi^2$  values obtained in the alternative fitting procedure are even lower than those shown in table 3, with the set OA1 having the lowest  $\chi^2$  value among all the sets. We have used the parameter sets HPA2 (that corresponds to minimum  $\chi^2$  in table 3), NA1 and OA1 of table 5 in our calculations on the hypernuclear properties presented in the next section.

## 4. Results and Discussions

### 4.1. $\Lambda$ single particle fields

The existence of the ground states of  $\Lambda$  hypernuclei is related to the single particle field ( $V_{\Lambda}$ ) for the  $\Lambda$  hyperon. In the SHF model the  $\Lambda N$  force contributes to the field  $V_{\Lambda}$  in proportional to various powers of  $\rho_N$ . It would be instructive to compare this quantity calculated within the Hartree-Fock theory ( $V_{\Lambda}^{HF}$ ) with those obtained with a phenomenological parameterization of ( $V_{\Lambda}^{ph}$ ) e.g. of Ref. [29] for hypernuclei with masses varying in a broad range. In Fig. 1, we show  $V_{\Lambda}^{HF}$  [calculated using Eq. (13) with the parameter set HPA2], for hypernuclei  ${}_{\Lambda}^{16}\text{O}$ ,  ${}_{\Lambda}^{40}\text{Ca}$ ,  ${}_{\Lambda}^{89}\text{Y}$ ,  ${}_{\Lambda}^{139}\text{La}$  and  ${}_{\Lambda}^{208}\text{Pb}$ . We also show in this figure the  $V_{\Lambda}^{ph}$  obtained within the parameterization of Ref. [29] for O, Ca and Pb systems - the corresponding potentials are actually taken from this reference. We notice that the central depths of potentials  $V_{\Lambda}^{HF}$  are around 29 MeV irrespective of the nuclear mass. In comparison,  $V_{\Lambda}^{ph}$  are somewhat less attractive. This result is in

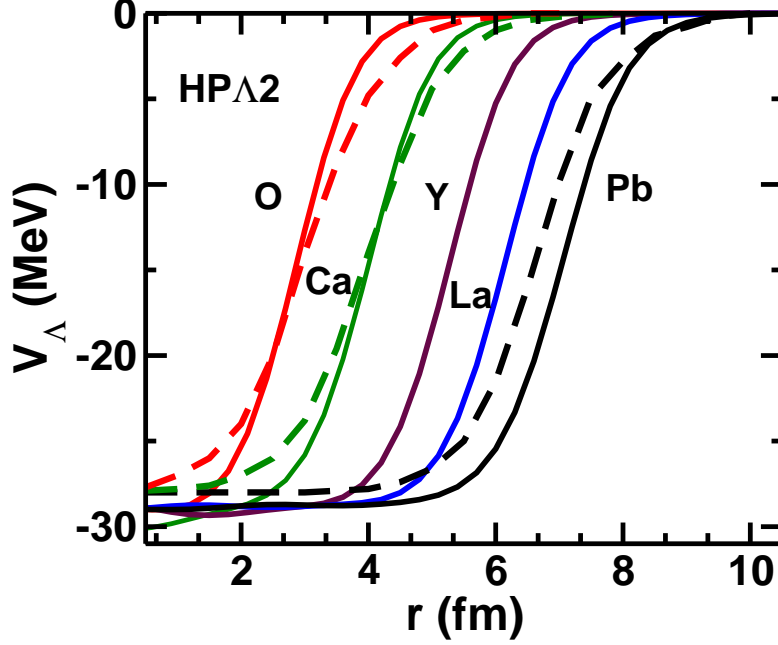


Figure 1: [color online] The solid lines show the coordinate space SHF mean field potential  $V_\Lambda$  in hypernuclei  $^{16}_\Lambda\text{O}$ ,  $^{40}_\Lambda\text{Ca}$ ,  $^{89}_\Lambda\text{Y}$ ,  $^{139}_\Lambda\text{La}$ , and  $^{208}_\Lambda\text{Pb}$  as marked near each line. The corresponding fields generated in an empirical Woods-Saxon parameterization (that are taken from Ref. [29]) are also shown for O, Ca and Pb nuclei by dashed lines near the lines showing the corresponding Hartree-Fock  $V_\Lambda$ .

contrast to that shown in Ref. [39] where the  $V_\Lambda^{HF}$  was found to be shallower than  $V_\Lambda^{ph}$ . Use of a different  $\Lambda N$  force could be one reason for this difference.

For the  $Pb$  nucleus, the  $V_\Lambda^{HF}$  extends to the larger values of  $r$  in comparison to  $V_\Lambda^{ph}$ . Similar trend was seen in Ref. [39]. This result has been attributed to the presence of the effective mass  $m^*$  in the HF equation which mocks up for some finite range effects in such approaches. This result is also in agreement with the observations made in Ref. [29] where it was shown that the presence of the  $\rho^2$  terms in the  $\Lambda$  potentials [Eqs. (13) and (14)] leads to an interaction with an increased half value radius as compared to that of the simple Woods-Saxon potential for heavier nuclei. However, in lighter systems the  $\rho^2$  dependent term of the potential seems to reduce the effective radius of the potential.

#### 4.2. Binding energies of $\Lambda$ single-particle states

In Fig. 2, we show a comparison of the calculated and the experimental  $\Lambda$  binding energies ( $B_\Lambda$ ) of  $1s$ ,  $1p$ ,  $1d$ ,  $1f$  and  $1g$  shells of a number of hypernuclei with masses ranging from 8 to 208. In these calculations, we have used SLy4 for the  $NN$  interaction and the parameter sets HPA2, NΛ1 and OΛ1 for the  $\Lambda N$  interaction. We note that there is an overall agreement between our calculations performed with HPA2 set and the experimental data in both the low mass and the high mass regions. However, sets

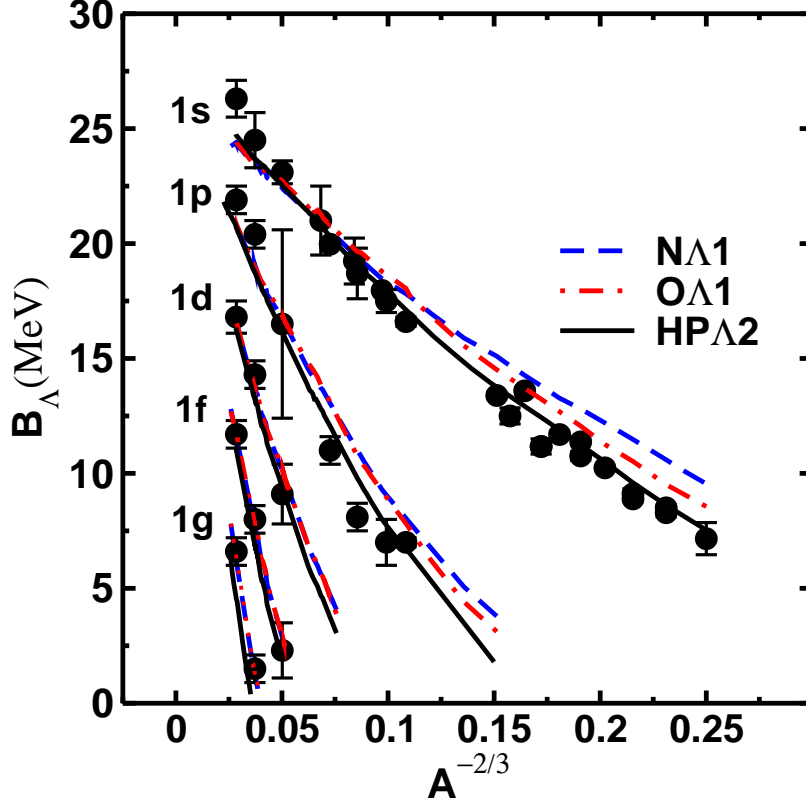


Figure 2: [color online] The comparison of experimental and calculated binding energies of  $1s$ ,  $1p$ ,  $1d$ ,  $1f$ , and  $1g$   $\Lambda$  states as a function of  $A^{-2/3}$  where  $A$  is the baryon number of the hypernucleus. In each case the solid, dashed and dashed-dotted lines correspond to the results obtained with  $\Lambda N$  interaction parameter sets of HP $\Lambda$ 2, N $\Lambda$ 1 and O $\Lambda$ 1, respectively.

O $\Lambda$ 1 and N $\Lambda$ 1 tend to overbind the  $1s$  and also to some extent the  $1p$   $\Lambda$  orbitals for lighter nuclei. This effect is relatively more stark with the set N $\Lambda$ 1. However, since the set HP $\Lambda$ 2 has been obtained by including the BE of the light nuclei as well in the fitting procedure, it is not surprising that it provides a better description of the  $B_\Lambda$  of the  $1s$  and  $1p$  orbitals of the lighter systems.

For heavier nuclei all the three sets describe the  $B_\Lambda$  equally well. In a marked contrast to the SHF results of Ref. [39], we observe the underbinding only for the  $1s$  single particle orbital of  $^{208}\text{Pb}$  hypernucleus. Moreover, even for this case the magnitude of the underbinding is much smaller in our calculation as compared that of Ref. [39]. In the SHF calculations presented in Ref. [46], underestimations of varying magnitudes were observed for the single particle energies of both  $s$  and  $p$  orbitals of the heavier systems with most of the  $\Lambda N$  interactions used. In the density dependent hadron field theory calculations of Ref. [5], the single particle energies were underpredicted by factors of up to 2.5 for hypernuclei with masses below  $^{28}_\Lambda\text{Si}$ . This was attributed to the

Table 6: The  $\Lambda$  effective mass (calculated at saturation density  $\rho_0$ ) and rms radii of ground state  $\Lambda$  orbitals of various hypernuclei.

SET	$m_{\Lambda}^*/m_{\Lambda}$	$r_{\Lambda}({}^9_{\Lambda}\text{Li})$ (fm)	$r_{\Lambda}({}^{12}_{\Lambda}\text{C})$ (fm)	$r_{\Lambda}({}^{16}_{\Lambda}\text{O})$ (fm)	$r_{\Lambda}({}^{28}_{\Lambda}\text{Si})$ (fm)	$r_{\Lambda}({}^{40}_{\Lambda}\text{Ca})$ (fm)	$r_{\Lambda}({}^{51}_{\Lambda}\text{V})$ (fm)	$r_{\Lambda}({}^{139}_{\Lambda}\text{La})$ (fm)	$r_{\Lambda}({}^{208}_{\Lambda}\text{Pb})$ (fm)
HPA1	0.88	3.16	2.96	2.98	3.09	3.27	3.42	4.10	4.75
HPA2	0.85	3.17	2.98	3.00	3.12	3.31	3.46	4.17	4.81
NA1	0.88	2.94	2.88	2.92	3.11	3.31	3.46	4.14	4.81
OA1	0.99	2.94	2.78	2.82	2.93	3.11	3.27	3.87	4.54
HPA3	0.86	3.19	2.98	2.99	3.09	3.27	3.43	4.11	4.75
HPA4	0.87	3.19	2.98	3.00	3.10	3.28	3.43	4.12	4.75
NA2	0.88	2.95	2.87	2.92	3.09	3.28	3.44	4.09	4.76
OA2	1.00	2.93	2.74	2.80	2.90	3.07	3.23	3.82	4.49

enhancement of surface effects in the lighter nuclei that are not accounted for properly in their calculations.

Looking at the fact that the parameter sets HPA2 provides a good overall description of the single particle spectra of the  $\Lambda$  hypernuclei which in some ways improves upon previous SHF calculations performed with different parameterizations, the predictions of our model can be used with relatively more confidence in calculations of the hypernuclear production cross sections via e.g.  $(\pi^+, K^+)$  [15], or  $(\gamma, K^+)$  [13, 14] reactions for those cases where experimental information may not be available about the binding energies of the  $\Lambda$  states.

In table 6, we show the effective  $\Lambda$  hyperon masses and the root mean square (rms) radii ( $r_{\Lambda}$ ) of the ground state  $\Lambda$  orbits of various hypernuclei calculated at the nuclear saturation density ( $n_0$ ) with various  $\Lambda N$  parameterizations obtained by us. This provides additional constraints on different parameter sets. First of all we note that  $m_{\Lambda}^*/m_{\Lambda}$  obtained with interactions having  $\gamma$  value of (1/3) (last 4 rows of this table) are slightly different from those involving  $\gamma = 1$ . The effective mass is largest with the parameter sets OA1 and OA2. Furthermore, these sets give the lowest  $r_{\Lambda}$  for various hypernuclei. It is also of interest to note that  $r_{\Lambda}$  calculated with our parameter sets are systematically larger than those obtained with Skyrme  $\Lambda N$  interactions of Ref. [46]. It should however be mentioned that some uncertainty in the rms radii originates from the choice of the NN potential which was also different in Ref. [46].

#### 4.3. Total binding energy per baryon of hypernuclei

Although the hyperon contribution to the total hypernuclear energy is relatively small, a systematic study of the total binding energies per baryon ( $BE/A$ ) of hypernuclei could be useful because it sheds light on the pattern of the stability of hypernuclei across the periodic table. Looking at the experimental data one notices that the  $BE/A$  of the medium mass hypernuclei is larger than those of the lighter and the heavier ones. This indicates that hypernuclei in this region may be more stable. In the SHF framework, the total binding energy of a hypernucleus of baryon number  $A$  can be obtained

Table 7: Binding energy per baryon number ( $BE/A$ ) of various known single lambda hypernuclei and corresponding values calculated by RMF method [79] are also listed for comparison.

Hypernuclei	$BE/A$ (MeV)	$BE/A$ (RMF) (MeV)	Hypernuclei	$BE/A$ (MeV)	$BE/A$ (RMF) (MeV)
$^9_\Lambda\text{Be}$	7.115	-	$^{62}_\Lambda\text{Ni}$	8.773	8.839
$^{10}_\Lambda\text{B}$	5.906	-	$^{63}_\Lambda\text{Ni}$	8.773	8.844
$^{14}_\Lambda\text{C}$	8.631	-	$^{64}_\Lambda\text{Ni}$	8.768	8.853
$^{14}_\Lambda\text{N}$	7.076	-	$^{65}_\Lambda\text{Ni}$	8.764	8.865
$^{15}_\Lambda\text{N}$	8.523	-	$^{86}_\Lambda\text{Kr}$	8.727	8.778
$^{20}_\Lambda\text{Ne}$	7.386	7.635	$^{87}_\Lambda\text{Kr}$	8.695	8.796
$^{21}_\Lambda\text{Ne}$	7.579	7.714	$^{87}_\Lambda\text{Rb}$	8.745	7.680
$^{24}_\Lambda\text{Mg}$	7.624	7.723	$^{88}_\Lambda\text{Rb}$	8.719	7.587
$^{27}_\Lambda\text{Al}$	8.184	-	$^{88}_\Lambda\text{Sr}$	8.754	7.657
$^{33}_\Lambda\text{S}$	8.666	-	$^{89}_\Lambda\text{Sr}$	8.734	7.564
$^{36}_\Lambda\text{S}$	8.579	8.637	$^{90}_\Lambda\text{Y}$	8.739	7.510
$^{37}_\Lambda\text{S}$	8.579	8.704	$^{90}_\Lambda\text{Zr}$	8.740	7.545
$^{38}_\Lambda\text{Ar}$	8.585	8.597	$^{91}_\Lambda\text{Zr}$	8.731	7.455
$^{39}_\Lambda\text{Ar}$	8.634	8.728	$^{92}_\Lambda\text{Mo}$	8.675	7.378
$^{48}_\Lambda\text{Ca}$	8.863	8.855	$^{93}_\Lambda\text{Mo}$	8.678	7.291
$^{49}_\Lambda\text{Ca}$	8.749	8.880	$^{112}_\Lambda\text{Sn}$	8.471	6.925
$^{50}_\Lambda\text{Ti}$	8.823	8.843	$^{113}_\Lambda\text{Sn}$	8.479	6.961
$^{51}_\Lambda\text{Ti}$	8.747	8.904	$^{114}_\Lambda\text{Sn}$	8.487	6.996
$^{52}_\Lambda\text{V}$	8.751	8.909	$^{115}_\Lambda\text{Sn}$	8.495	7.032
$^{54}_\Lambda\text{Fe}$	8.725	8.774	$^{116}_\Lambda\text{Sn}$	8.502	7.030
$^{55}_\Lambda\text{Fe}$	8.715	8.897	$^{117}_\Lambda\text{Sn}$	8.509	7.028
$^{58}_\Lambda\text{Ni}$	8.666	8.856	$^{118}_\Lambda\text{Sn}$	8.516	7.027
$^{59}_\Lambda\text{Ni}$	8.705	8.847	$^{119}_\Lambda\text{Sn}$	8.523	7.026
$^{60}_\Lambda\text{Ni}$	8.738	8.841	$^{120}_\Lambda\text{Sn}$	8.530	7.026
$^{61}_\Lambda\text{Ni}$	8.763	8.838	$^{121}_\Lambda\text{Sn}$	8.538	7.026

from Eq. (22).

In Tables (7) and (8) we present the results of our SHF calculations (done with the HPA2 force) for  $BE/A$  for 73 hypernuclei with masses in the range of 9 to 211. The results obtained with sets N $\Lambda$ 1 and O $\Lambda$ 1 are almost the same. We note that for the lighter systems ( $A < 28$ ), the stability of a hypernucleus depends on that of the nucleus where a neutron is replaced by the hyperon. For example,  $^9_\Lambda\text{Be}$  is more stable than  $^9_\Lambda\text{B}$ , and  $^{14}_\Lambda\text{C}$  is more stable than  $^{14}_\Lambda\text{N}$ . For hypernuclei with baryon number in the range of 30-95 the  $BE/A$  is around 8.7 MeV and it decreases gradually with further increase in the mass number. For comparison purpose the results of a relativistic mean field (RMF) model taken from Ref. [79] are also presented wherever available. RMF results for the  $BE/A$  are given only in this reference. We note that that for nuclei with baryon number in excess of 87 the RMF model underbinds the hypernuclei. However, the difference seen between SHF and RMF energies could possibly result from the differences in the nuclear energies predicted by the two models. Therefore, one should be careful in

Table 8: Same as table 7.

Hypernuclei	BE/A (MeV)	BE/A (RMF) (MeV)	Hypernuclei	BE/A (MeV)	BE/A (RMF) (MeV)
$^{122}_{\Lambda}\text{Sn}$	8.545	7.026	$^{141}_{\Lambda}\text{Ce}$	8.204	6.874
$^{123}_{\Lambda}\text{Sn}$	8.551	7.027	$^{141}_{\Lambda}\text{Pr}$	8.337	6.823
$^{124}_{\Lambda}\text{Sn}$	8.554	7.028	$^{142}_{\Lambda}\text{Pr}$	8.339	6.855
$^{125}_{\Lambda}\text{Sn}$	8.552	7.030	$^{142}_{\Lambda}\text{Nd}$	8.321	6.800
$^{132}_{\Lambda}\text{Sn}$	8.415	7.066	$^{143}_{\Lambda}\text{Nd}$	8.325	6.834
$^{133}_{\Lambda}\text{Sn}$	8.391	7.074	$^{144}_{\Lambda}\text{Sm}$	8.280	6.753
$^{136}_{\Lambda}\text{Xe}$	8.392	6.949	$^{145}_{\Lambda}\text{Sm}$	8.289	6.790
$^{137}_{\Lambda}\text{Xe}$	8.381	6.968	$^{209}_{\Lambda}\text{Pb}$	7.886	6.726
$^{138}_{\Lambda}\text{Ba}$	8.375	6.886	$^{210}_{\Lambda}\text{Bi}$	7.854	6.711
$^{139}_{\Lambda}\text{Ba}$	8.369	6.911	$^{210}_{\Lambda}\text{Po}$	7.826	6.689
$^{140}_{\Lambda}\text{La}$	8.362	6.893	$^{211}_{\Lambda}\text{Po}$	7.833	6.696
$^{140}_{\Lambda}\text{Ce}$	8.352	6.845			

interpreting the comparison of the results produced by these two mean field models.

#### 4.4. Properties of a neutron star

In order to calculate neutron-star properties, it is necessary to have an Equation of State (EOS) linking pressure to the total energy density of the dense matter. At densities closer to the nuclear saturation density ( $n_0 = 0.16 \text{ fm}^{-3}$ ), the matter is mostly composed of neutrons, protons and leptons (electrons and muons) in  $\beta$  equilibrium. As density increases, new hadronic degrees of freedom may appear. Hyperons are one of them as the equilibrium conditions in neutron stars make the formation of hyperons energetically favorable. The role of hyperons on the neutron star properties has been studied by several authors (see, e.g. Refs. [80, 81, 82, 83, 84, 85, 86, 87, 88]).

In this section, we employ the best fit  $\Lambda N$  interactions obtained by us to discuss the implications of hyperons on the EOS and the structure of neutron stars. Unlike several other authors, we have included only the  $\Lambda$  hyperons into our calculations as this study is restricted to testing the interactions obtained in this work. In that sense our work may appear to be less complete in comparison to many previous studies where include other hyperons were included as well. Nevertheless, in all likelihood the  $\Sigma N$  interaction is repulsive because no stable  $\Sigma$  hypernucleus other than that of mass 4, is known to exist. Therefore,  $\Sigma$  appears at much higher densities [87] as compared to  $\Lambda$ . The  $\Xi$  hyperon, on the other hand, could appear at densities comparable to those of  $\Lambda$ . However, there is considerable amount of uncertainty about the strength of  $\Xi N$  interaction as no bound  $\Xi$  hypernucleus has been detected so far. The threshold of the appearance of the  $\Xi$  hyperons is pushed to higher densities with increasing  $\Xi N$  potential.

In our calculations of the EOS, we have closely followed the methods reported in Refs. [89, 90, 47, 49]. To our energy density functional [Eq. (1)] we have also added a contribution corresponding to the  $\Lambda\Lambda$  interaction as at higher densities the results are sensitive to this term, for which the energy density functional is taken from Ref. [47]



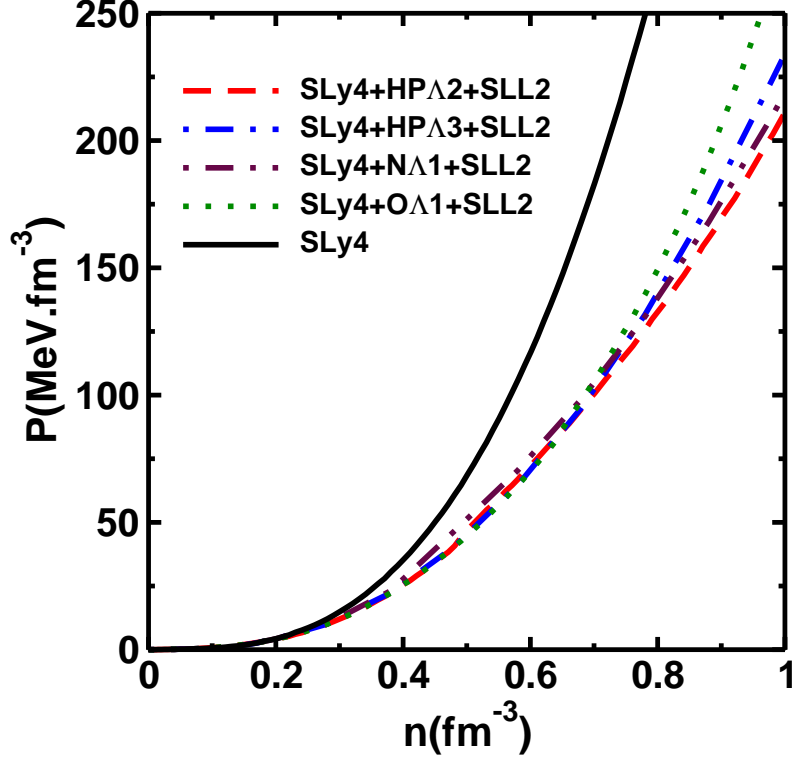


Figure 3: [color online] The equation of state (pressure as a function of baryon number density) obtained by using  $\Lambda N$  interactions  $HP\Lambda 2$  (dashed line),  $HP\Lambda 3$  (dashed-dotted line),  $N\Lambda 1$  (dashed-double dotted line) and  $O\Lambda 1$  (dotted line).

with parameters corresponding to their set SLL2. The energy density includes the rest energies of the matter constituents. The leptonic contribution to the energy density is calculated as discussed in Refs. [47, 49] (see also [91]). For this sector the energy densities corresponding to electrons and muons are written as

$$\mathcal{E}_l = \frac{1}{\pi^2} \int_0^{k_f^l} k^2 \sqrt{k^2 + m_l^2} dk, \quad (25)$$

where  $l = e$  (electron) or  $\mu$  (muon) and  $k_f^l$  is the corresponding Fermi momentum. For a given baryon density the values of the Fermi momenta for neutrons, protons,  $\Lambda$ , electron and muon can be obtained by requiring that neutron star matter is in  $\beta$  equilibrium. This leads to the following equations for the equality of the chemical potentials (represented by  $\mu$  in the following)

$$\begin{aligned} \mu_n - \mu_p &= \mu_e, & \mu_\mu &= \mu_e \\ \mu_n + m_n &= \mu_\Lambda + m_\Lambda, \end{aligned} \quad (26)$$

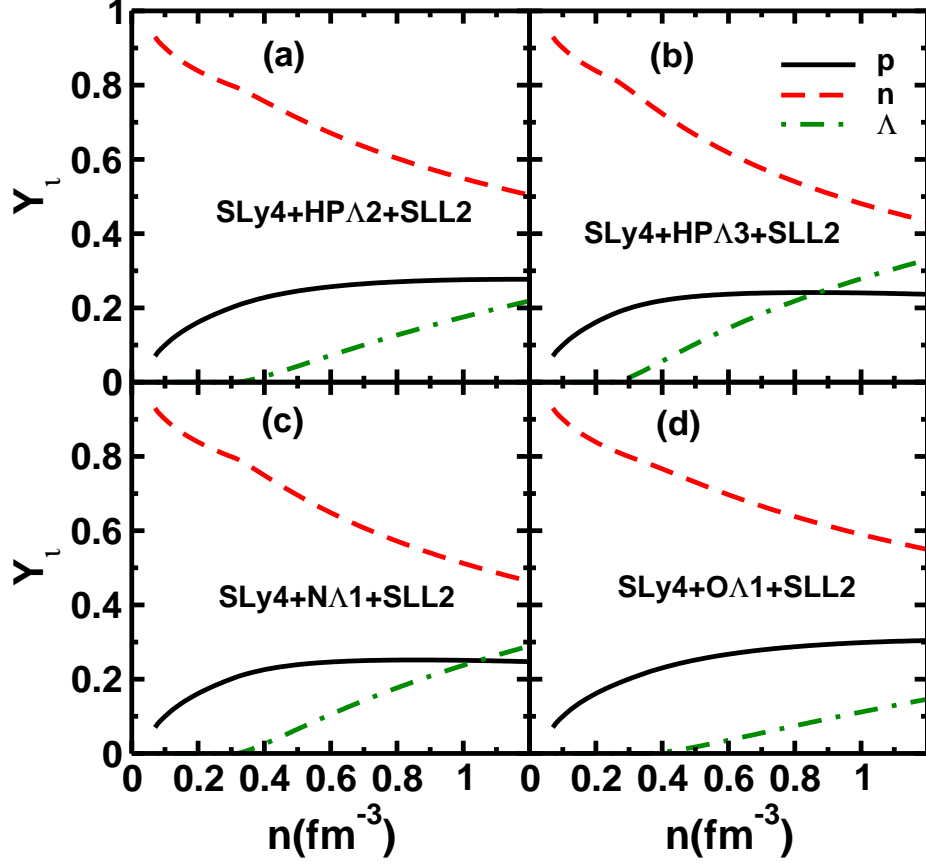


Figure 4: [color online] Particle fractions obtained with using  $\Lambda N$  interactions HP $\Lambda$ 2 (a), HP $\Lambda$ 3 (b), N $\Lambda$ 1 (c) and O $\Lambda$ 1 (d).

where chemical potentials are defined as

$$\mu_j = \frac{\partial \mathcal{E}}{\partial n_j} \quad (27)$$

where  $\mathcal{E}$  is total energy density and  $n_j$  the particle number density.

The total baryon number density is  $n_b = n_n + n_p$  and the charge neutrality requires  $n_p = n_e + n_\mu$ , where  $n_e$  and  $n_\mu$  are the number densities of electrons and muons, respectively. These equations combined with Eq. 26 give the particle fraction  $Y_j = \frac{n_j}{n_b}$ . The EOS is defined by the expressions

$$\rho(n_b) = \frac{\mathcal{E}(n_b)}{c^2}, \quad P(n_b) = n_b^2 \frac{d(\mathcal{E}/n_b)}{dn_b}, \quad (28)$$

where  $\rho(n_b)$  is the mass density of the matter.

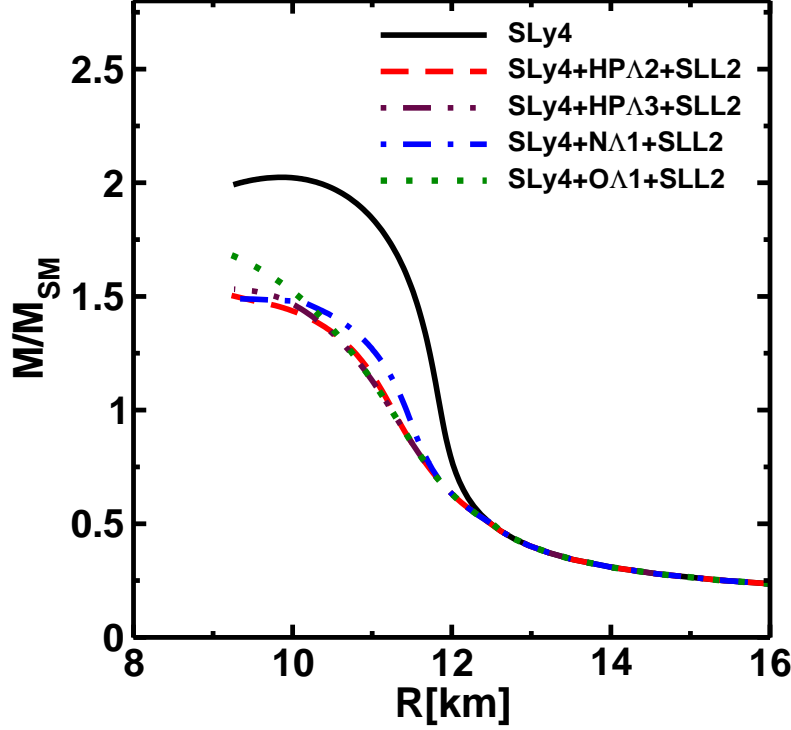


Figure 5: [color online] Mass radius relation for neutron stars obtained with EOS shown in Fig. 3 with interactions HPA2, HPA3, NA1 and OΛ1.

In Fig. 3 we show the equation of state calculated with  $\Lambda N$  interactions HPA2, HPA3, NA1, and OΛ1. It is to be noted that in each case the inclusion of hyperons makes the EOS much softer with respect to that of the pure nucleonic case. Since hyperons can be accommodated in the lower momentum states, their kinetic energies are decreased which leads to the softening of the EOS. We see that the degree of softness of the EOS obtained with HPA2 and NA1 interactions are almost identical. However, with HPA3 the softness is comparatively smaller and with OΛ1 the softening of the EOS is relatively the lowest.

In Fig. 4, we show the particle fraction  $Y_i$  as a function of the total baryonic density. It is clear from this figure that neutrons are by far the most dominant object of the matter. One further notices that while in panels (a), (b) and (c)  $\Lambda$  hyperon appears at about twice the nuclear saturation density, in panel (d) they start only after about  $2.5n_0$ . They are also less numerous in this case as compared to those in other 3 panels. This is the consequence of the fact that with the interaction OΛ1 the softness introduced to the nucleon only EOS is the least. The rise of hyperon fraction, after their formation, is quickest with HPA3 and NA1 interactions as compared to that seen with other interactions.

Further consequences of the different nature of the EOS softening with the intro-

duction of the  $\Lambda$  hyperon with different  $\Lambda N$  interactions can be seen on the their effect on the neutron star masses. To obtain the relation between neutron star mass and its radius, we have solved the Tolmann-Oppenheimer-Volkoff equation

$$\begin{aligned} \frac{dP}{dr} &= -\frac{G\mathcal{E}(r)M(r)}{r^2c^2} \left[ 1 + \frac{P(r)}{\mathcal{E}(r)} \right] \left[ 1 + \frac{4\pi r^3 P(r)}{M(r)c^2} \right] \\ &\times \left[ 1 - \frac{2GM(r)}{rc^2} \right]^{-1}, \end{aligned} \quad (29)$$

and

$$\frac{dM(r)}{dr} = \frac{4\pi r^2 \mathcal{E}(r)}{c^2}, \quad (30)$$

where  $P$ ,  $\mathcal{E}$ , and  $M$  are the pressure, energy density and gravitational mass of the neutron star, respectively. These quantities depend on the distance  $r$  from the center. Eqs. 29 and 30 can be solved from the knowledge of the initial value of the pressure  $P$  at the center ( $r=0$ ) and using  $M(0) = 0$  and the relationship of  $P$  and  $\mathcal{E}$  (EOS).

The predicted masses of the neutron star [measured in solar masses  $M_\odot$ ] as a function of radius (in kilometer[km]) are shown in Fig. 5 using EOS of Fig. 3. We note that with EOS obtained with interactions HPA2, HPA3, and N $\Lambda$ 1 maximum neutron star mass is similar (around  $1.5 M_\odot$ ). In Fig. 5,  $M_\odot$  is depicted as  $M_{SM}$ . However, with the EOS corresponding to the interaction O $\Lambda$ 1 the maximum mass is about  $1.75 M_\odot$ . This result can be understood from the fact that a stiffer EOS leads to a larger neutron star maximum mass. It may be mentioned here that if  $\Lambda\Lambda$  interaction is switched off the maximum neutron star mass fails to reach to even its "canonical" value of  $1.4 M_\odot$ .

## 5. Summary and conclusions

In summary, we have used an extended Skyrme Hartree-Fock model to describe the properties of the  $\Lambda$  hypernuclei. New parameterizations for the Skyrme type  $\Lambda N$  force have been obtained by fitting to the experimental binding energies of about 20  $\Lambda$  hypernuclear orbitals with the baryon number ranging from 8 to 208 (the best fit parameter set is termed at HPA2). We have also performed the fittings by excluding the binding energies of nuclei with masses below 16. In this case two sets of parameters were obtained: in the first one (termed as N $\Lambda$ 1) the binding energies of the  ${}^{16}_\Lambda\text{O}$  hypernucleus were excluded but those of the  ${}^{16}_\Lambda\text{N}$  hypernucleus measure recently in a  $(e, e'K^+)$  experiment were include in the fitting procedure, while in the second one (termed as O $\Lambda$ 1) the reverse was done. The fitting method uses an elegant  $\chi^2$  minimization method based on the simulated annealing method.

These three sets of the best fit parameters were used to calculate the binding energies of  $1s$ ,  $1p$ ,  $1d$ ,  $1f$  and  $1g$  shells of a number of hypernuclei. We find that calculations performed with the set HPA2 provide the best agreement with the experimental binding energies in the entire range of mass values and for all the orbitals. The set O $\Lambda$ 1 produces binding energies, which overestimate somewhat the corresponding experimental data of the  $1s$  and to a lesser extent of the  $1p$  orbitals for the lighter nuclei.

This overestimation is larger in case of the set NA1. However, all the three sets produce equally good agreement with the experimental data for heavier nuclei for all the orbitals.

Except for one case [ $1s$  orbital of  $^{208}\text{Pb}$  nucleus], our calculations do not underbind the heavier systems. This is a marked improvement over the similar previous Hartree-Fock studies of  $\Lambda$  hypernuclei where binding energies of orbitals of several heavier nuclei were underpredicted. Furthermore, the root mean square radii of heavier systems are predicted to be larger than those obtained in previous SHF calculations done with different  $\Lambda N$  forces.

We made a systematic study of the mass dependence of the total binding energy per baryon of 73  $\Lambda$  hypernuclei spanning the entire range of the periodic table. It is observed that hypernuclei with masses in the range of 30-95 are more stable than those lying in other regions. For lighter systems some of the hypernuclei are more stable than their immediate neighbors on both sides.

We have also tested our best fit  $\Lambda N$  interactions to investigate the role of hyperons in the neutron star sector. In these studies, we used the same  $NN$  effective interaction ( $SLy4$ ) together with HPA2, HPA3, NA1 and OA1 effective  $\Lambda N$  interactions. Inclusion of the  $\Lambda\Lambda$  interaction was also found to be necessary in these studies - we took the corresponding effective Hamiltonian from the work of Lansky [94]. It is noted that inclusion of the  $\Lambda$  hyperon makes the neutron star equation of state softer. However, while the sets HPA2, HPA3 and NA1 lead the softness of the similar magnitude, that obtained with the set OA1 is lesser. Furthermore, with this set the  $\Lambda$  hyperon appear at a relatively higher density and are relatively less numerous as compared to other three sets.

The maximum neutron star mass obtained with sets HPA2, HPA3 and NA1 is about  $1.5M_{\odot}$ , while that with the set OA1 is  $1.75M_{\odot}$ . This is the direct consequence of the relatively stiffer EOS in this case. We remark that these results obtained with our best fit  $\Lambda N$  effective interactions reproduce quantitatively all the features that have been observed in several different models such as non-relativistic Brueckner-Hartree-Fock and relativistic mean field calculations. Nevertheless, an explanation of some of the recent neutron star observations [92] such as pulsar PSR J1614-2230 with a mass of  $1.97 \pm 0.04M_{\odot}$  is still beyond the scope of the present Skyrme type of model unless the EOS is even stiffer than what has been achieved with the interaction OA1.

One of the authors (NG) would like to thank the theory division of the Saha Institute of Nuclear Physics, Kolkata for financial support and hospitality during a visit. She is also grateful to Himachal Pradesh University, Shimla for providing her a Ph.D. scholarship. Useful discussions with Prof. A. W. Thomas are gratefully acknowledged. This work has been partly supported by the University of Adelaide and the Australian Research Council through grant FL0992247(AWT).

## References

- [1] R. H. Dalitz and A. Gal, Ann. Phys. **116** (1978) 167.
- [2] B. Povh, Progr. Part. Nucl. Phys., **18** (1987) 183.

- [3] Y. Yamamoto, T. Matoba, H. Himeno, K. Ikeda, and S. Nagata, Prog. Theor. Phys. Suppl. **117** (1994) 361.
- [4] B. F. Gibson and E. V. Hungerford III, Phys. Rep. **257** (1995) 349.
- [5] C. M. Keil, F. Hoffmann, and H. Lenske, Phys. Rev. C **61** (2000) 064309.
- [6] A. Gal, Prog. Theor. Phys. Suppl. **156** (2004) 1.
- [7] O. Hashimoto and H. Tamura, Prog. Part. Nucl. Phys. **57** (2006) 564.
- [8] K. Saito, K. Tsushima, and A. Thomas, Prog. Part. Nucl. Phys. **58** (2007) 1.
- [9] P. Finelli, N. Kaiser, D. Vretenar and W. Weise, Nucl. Phys. A **831** (2009) 163.
- [10] C. B. Dover, L. Ludeking, G. E. Walker, Phys. Rev. C **22** (1980) 2073.
- [11] R. Hausmann and W. Weise, Nucl. Phys. A **491** (1989) 598
- [12] H. Bando, T. Motoba and J. Zofka, Int. J. Mod. Phys. A **5** (1990) 4021.
- [13] R. Shyam, H. Lenske and U. Mosel, Phys. Rev. C **77** (2008) 052201.
- [14] R. Shyam, K. Tsushima and A. W. Thomas, Phys. Lett. B **676** (2009) 51.
- [15] S. Bender, R. Shyam and H. Lenske, Nucl. Phys. A **839** (2010) 51.
- [16] F. Weber, Prog. Part. Nucl. Phys., **54** (2005) 193; J. Schaffner-Bielich, J. Phys. G **31** (2005) S651.
- [17] S. R. Beane, P. F. Bedaque, A. Parreno, and M. J. Savage, Nucl. Phys. A **747** (2005) 55.
- [18] M. Rufa, J. Schaffner, J. Maruhn, H. Stocker, W. Greiner, P. G. Reinhard, Phys. Rev. C **42** (1990) 2469.
- [19] N. K. Glendenning, D. Von-Eiff, M. Haft, H. Lenske, and M. K. Weigel, Phys. Rev. C, **48** (1993) 889.
- [20] J. Mares and B.K. Jennings, Phys. Rev. C **49** (1994) 2472.
- [21] R. J. Lombard, S. Marcos and J. Mares, Phys. Rev. C **51** (1995) 1784.
- [22] D. Vretenar, W. Poschl, and G. A. Lalazissis, and P. Ring, Phys. Rev. C, **57** (1998) 1060.
- [23] H. Müller, Phys. Rev. C **59** (1999) 1405.
- [24] P. Papazoglou, S. Schramm, J. Schaffner-Bielich, H. Stöcker, W. Greiner, Phys. Rev. C **57** (1998) 2576.
- [25] K. Tsushima, K. Saito, J. Heidenbauer, A. W. Thomas, Nucl. Phys. A **630** (1998) 691.

- [26] P. M. Guichon, A. W. Thomas, and K. Tsushima, Nucl. Phys. **A 814** (2008) 66.
- [27] D. J. Millener, Nucl. Phys. **A 835** (2010) 11c and references therein.
- [28] A. Bouyssy and J. Hüfner, Phys. Lett. **B 64** (1976) 276; A. Bouyssy, Phys. Lett. **B 84** (1979) 41.
- [29] D. J. Millener, C. B. Dover, and A. Gal, Phys. Rev. C **38** (1988) 2700.
- [30] S. Iwao, Prog. Theo. Phys., **46** (1971) 1407.
- [31] M. Grypeos, G. Lalazissis and S. Massen, Nucl. Phys. **A 450** (1986) 283c.
- [32] C. Samanta, P. Roy Chowdhury and D. N. Basu, J. Phys. G:Nucl. Part. Phys. **32** (2006) 363.
- [33] D. Vautherin and D. M. Brink, Phys. Lett. **32B** (1970) 149; D. Vautherin and D. M. Brink, Phys. Rev. C **5** (1972) 626; D. Vautherin, Phys. Rev. C **7** (1973) 296.
- [34] C. B. Dover and Nguyen Van Giai, Nucl. Phys. **A 190** (1972) 373;
- [35] M. Beiner, H. Flocard, Nguyen Van Giai, and P. Quentin, Nucl. Phys. **A 238** (1975) 29.
- [36] M. Rayet, Ann. of Phys. **102** (1976) 226.
- [37] M. Rayet, Nucl. Phys. **A 367** (1981) 381.
- [38] Y. Yamamoto and H. Bando, Prog. Theo. Phys. Suppl. **81** (1985) 42; Y. Yamamoto, T. Motoba, H. Himeno, K. Ikeda and S. Nagata, Prog. Theo. Phys. Suppl. **117** (1994) 361.
- [39] J. Cugnon, A. Lejeune, and H. J. Schulze, Phys. Rev. C **62** (2000) 064308.
- [40] I. Vidaña, A. Polls, A. Ramos, and H.-J. Schulze, Phys. Rev. C **64** (2001) 044301.
- [41] Xian-Rong Zhou, J.-J. Schulze, H. Sagawa, Chen-Xu Wu, En-Guang Zhao, Phys. Rev. C **76** (2007) 034312.
- [42] Xian-Rong Zhou, A. Polls, H.-J. Schulze, and I. Vidaña, Phys. Rev. C **78** (2008) 054306.
- [43] H.-J. Schulze, Nucl. Phys. **A 835** (2010) 19.
- [44] Y. Yamamoto, H. Bando and J. Zofka, Prog. Theor. Phys. **80** (1988) 757.
- [45] F. Fernandez, T. Lopez-Arias and C. Prieto, Z. Phys. A **334** (1989) 349.
- [46] D. E. Lansky and Y. Yamamoto, Phys. Rev. C **55** (1997) 2330.
- [47] L. Mornas, Eur. Phys. J. A **24** (2005) 293.

- [48] E. Chabanat, P. Bonche, P. Haensel, J. Meyer, and R. Schaeffer, Nucl. Phys. A **635** (1998) 231.
- [49] B. K. Agrawal, S. K. Dhiman, and R. Kumar, Phys. Rev. C **73** (2006) 034319.
- [50] S. S. Chandel, S. K. Dhiman, and R. Shyam, Phys. Rev. C **68** (2003) 054320.
- [51] J. R. Stone and P. G. Reinhard, Prog. Nucl. Part. Phys. **58** (2007) 587.
- [52] H. S. Green, Nucl. Phys. **57** (1964) 483.
- [53] A. R. Bodmer and Q. N. Usmani, Nucl. Phys. A **450** (1986) 257c
- [54] S. Takeuchi and K. Shimizu, Phys. Lett. B **179** (1986) 197.
- [55] Y. Akaishi et al., Phys. Rev. Lett. **84** (2000) 3539.
- [56] R. Brockmann and W. Weise, Nucl. Phys. A **355** (1981) 365.
- [57] H. J. Pirner, B. Povh, Phys. Lett. B **114** (1982) 308.
- [58] B. K. Agrawal, S. Shlomo, and V. K. Au, Phys. Rev. C **72** (2005) 014310.
- [59] D. H. Davis, Nucl. Phys. A **754** (2005) 3c.
- [60] T. Hasegawa and et al., Phys. Rev. Lett. **74** (1995) 224.
- [61] T. Hasegawa and et al., Phys. Rev. C **53** (1996) 1210.
- [62] Y. Miyura et al., Acta Phys. Polon., **B35** (2004) 1019.
- [63] M. Ahmed et al., Phys. Rev. C **68** (2003) 064004.
- [64] H. Hotchi and et al., Phys. Rev. C **64** (2001) 044302.
- [65] S. Ajimura et al., Phys. Rev. Lett. **86** (2001) 4255.
- [66] H. Kohri et al., Phys. Rev. C **65** (2002) 034607.
- [67] F. Cusanno and et al., Phys. Rev. Lett. **103** (2009) 202501.
- [68] M. Ukai and et al., Phys. Rev. Lett. **93** (2004) 232501.
- [69] O. Hashimoto et al., Nucl. Phys. A **639** (1998) 93c.
- [70] R. Bertini and et al., Phys. Lett. B, **B 83** (1979) 306.
- [71] H. Tamura et al., Prog. Theo. Phys. **117** (1994) 1.
- [72] R. E. Chrien and et al., Nucl. Phys. A **478** (1988) 705.
- [73] P. H. Pile and et al., Phys. Rev. Lett. **66** (1991) 2585.
- [74] S. Kirkpatrik, J. Stat. Phys. **34** (1984) 975.



- [75] L. Ingber, Math. Comput. Modeling **12** (1989) 967.
- [76] B. Cohen, Master's Thesis, Tel-Aviv University (1994) (unpublished).
- [77] T. Burvenich, D. G. Madland, J. A. Maruhn and P. -G. Reinhard, Phys. Rev. C **65** (2002) 044308.
- [78] T. Burvenich, D. G. Madland, and P. G. Reinhard, Nucl. Phys. **A 744** (2004) 92.
- [79] Lan Mi-Xiang, Li Lei, Ning Ping-Zhi, Chinn. Phys. Lett. **26** (2009) 072101.
- [80] N. K. Glendenning, Astrophys. J. **293** (1985) 470.
- [81] N. K. Glendenning and S. Moszkowski, Phys. Rev. Lett. **67** (1991) 2414.
- [82] S. Balberg and A. Gal, Nucl. Phys. **A 625** (1997) 435.
- [83] M. Baldo, G. F. Burgio and H.-J. Schulze, Phys. Rev. C **61** (2000) 055801.
- [84] I. Vidana, A. Polls, A. Ramos, L. Engvik, and M. Hjorth-Jensen, Phys. Rev. C **62** (2000) 035801.
- [85] H.-J. Schulze, A. Polls, A. Ramos and I. Vidana, Phys. Rev. C **73** (2006) 058801.
- [86] H.-J. Schulze, and T. Rijken, Phys. Rev. C **84** (2011) 035801.
- [87] S. Weissenborn, D. Chatterjee and J. Schaffner-Bielich, Nucl. Phys. **A 881** (2012) 62.
- [88] D. L. Whittenbury, J. D. Carroll, A. W. Thomas, K. Tsushima, and J. R. Stone, arXiv:1204.2614 [nucl-th].
- [89] E. Chabanat, P. Bonche, P. Haensel, J. Meyer and R. Schaeffer, Nucl. Phys. **A 627** (1997) 710.
- [90] J. Rikowska Stone, J. C. Miller, R. Koncewicz, P. D. Stevenson, and M. R. Strayer, Phys. Rev. C **68** (1993) 034324.
- [91] G. Baym, C. Pethick and P. Sutherland, Astrophys. J. **170** (1971) 299.
- [92] P. B. Demorest, T. Pennucci, S. M. Ransom, M. S. E. Roberts and J. W. T. Hessels, Nature **467** (2010) 1081.
- [93] B. F. Gibson, A. Goldberg, and M. S. Weiss, Phys. Rev. **181** (1969) 1486.
- [94] D. E. Lanskoy, Phys. Rev. C **58** (1998) 3351.